Buckling characteristics and static studies of multilayered magneto-electro-elastic plate

M.C. Kiran and S.C. Kattimani[*]

Department of Mechanical Engineering, National Institute of Technology Karnataka, Surathkal 575025, India

Abstract. This article deals with the buckling behaviour of multilayered magneto-electro-elastic (MEE) plate subjected to uniaxial and biaxial compressive (in-plane) loads. The constitutive equations of MEE material are used to derive a finite element (FE) formulation involving the coupling between electric, magnetic and elastic fields. The displacement field corresponding to first order shear deformation theory (FSDT) has been employed. The in-plane stress distribution within the MEE plate existing due to the enacted force is considered to be equivalent to the applied in-plane compressive load in the pre-buckling range. The same stress distribution is used to derive the potential energy functional. The non-dimensional critical buckling load is accomplished from the solution of allied linear eigenvalue problem. Influence of stacking sequence, span to thickness ratio, aspect ratio, load factor and boundary condition on critical buckling load and their corresponding mode shape is investigated. In addition, static deflection of MEE plate under the sinusoidal and the uniformly distributed load has been studied for different stacking sequences and boundary conditions.

Keywords: magneto-electro-elastic plate; FSDT; finite element; buckling analysis; static studies; in-plane loads

1. Introduction

Recently, an increasing application of MEE composites has attracted many researchers in the field of aerospace structures, surface sensitive electronic probes, stress monitoring devices, electrically and magnetically tuneable high frequency oscillators, sensors, and actuators. The MEE composite is composed of two distinct phases of the piezoelectric and magnetostrictive material. The combination of two such phases will induce a new product property (van Suchtelen 1972) which is absent in their individual constituents. Such composites facilitate energy conversion between electric, magnetic and elastic quantities. The conversion of various form of energy within the composite makes it most suitable for multifunctional devices. With the first production of MEE composite (Boomgaard and Bom 1978) by unidirectional solidification from eutectic compositions, a numerous theoretical study pertaining to free vibration, static behaviour, non-linear and large-deflection studies of MEE composites were reported. Pan and his co-researchers (Pan 2001, Pan and Heyliger 2002, 2003, Pan and Han 2005) carried out extensive research to assess the structural behaviour of magneto-electro-elastic plates. Studies related to free vibration of MEE plate were thoroughly investigated to predict their corresponding natural frequencies. A wide spectrum of techniques and theories including analytical solutions, different shear deformation theories, FE models and recently non local theory etc., has helped in understanding the free vibration behaviour of multilayered and functionally graded MEE plates (Buchnan 2004, Ramirez *et al.* 2006, Shooshtari and Razavi 2016, Ke *et al.* 2014, Xin and Hu 2015, Milazzo 2016, Chen *et al.* 2014).

Consequently, the deformation of MEE plate subjected to an applied load and their corresponding strain and stress vectors are evaluated in static studies. In addition, the effect of applied load on electric and magnetic quantities is clearly assessed (Lage *et al.* 2004, Moita *et al.* 2009, Liu *et al.* 2016, Bhangale and Ganesan 2006, Viun *et al.* 2016, Ray *et al.* 1994, Zhou *et al.* 2016, Vinyas and Kattimani 2017a, 2017b, Wu *et al.* 2010). The 1-3 piezoelectric composite patch on the substrate MEE structure was used to control the geometrical nonlinear vibrations by Kattimani and Ray (2015, 2014a, 2014b). Liu *et al.* (2016b) obtained high order solutions for MEE plate with non-uniform materials. A transient analysis was carried out on a conducting crack in a MEE half-space by Rogowski (2015). The wave propagation characteristics of MEE functionally graded nano-plate was analysed by Ebrahimi *et al.* (2016) using the higher order theory along with non-local Erignen's theory accounting the small-scale influence. Also, Ebrahimi and Barati (2016b) investigated the free vibration characteristics of smart shear deformable plates made of porous magnetoelectro-elastic functionally graded (MEE-FG) materials. Ebrahimi and Barati (2016a, 2017) proposed a unified formulation for dynamic analysis of nonlocal heterogeneous nanobeams in hygro-thermal environment.

The buckling behaviour of laminated composites and MEE structure were subsequently reported by a few researchers. A discrete FE model was developed by Moita *et al.* (1996) using higher-order theory to analyse the buckling behaviour of multi-laminated composite structures. The free

---

*Corresponding author, Assistant Professor
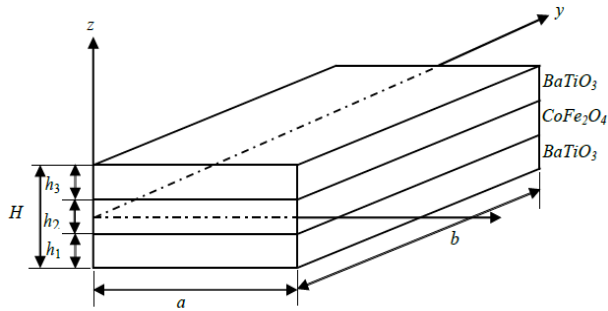E-mail: subhaskatti@gmail.com, sck@nitk.ac.in

Fig. 1 Schematic representation of multilayered MEE plate

Fig. 2 Schematic representation of uniaxial and biaxial compression on MEE plate

vibration and buckling characteristics of laminated composite plates were analysed by Luccioni *et al.* (1998) using classical plate theory and FSDT. Bouzza *et al.* (2016) presented a refined hyperbolic shear deformation theory for thermal buckling of laminated plates. Vuksanović (2000) carried out the linear buckling analysis of laminated composite plates by implementing the higher-order discrete model. Grover *et al.* (2014) developed a computationally efficient C_0 FE model for the analysis of sandwich and laminated composite plates. The bending, buckling and vibration behaviour of functionally graded plates was investigated using a new sinusoidal shear deformation theory by Thai and Vo (2013). Kulkarni *et al.* (2015) introduced inverse trigonometric shear deformation theory to study the bending and buckling characteristics of functionally graded plates. Under the thermal environment, Kumarvel *et al.* (2007) analysed the buckling characteristics of layered and multiphase MEE beam. Lang and Xuewu (2013) analysed the buckling behaviour of functionally graded magneto-electro-thermo-elastic (METE) circular cylindrical shell. Buckling characteristics of MEE plate resting on an elastic foundation was studied by Li (2014). Under magneto-electro-thermo-mechanical (METM) loads, Ansari (2016) investigated the buckling and post-buckling behaviour of METE nanoplates. Ebrahimi *et al.* (2016c) developed a nonlocal four-variable refined plate theory to examine the buckling behaviour of nanoplates made of FG-MEE materials resting on Winkler-Pasternak foundation. Jamalpoor *et al.* (2016) analysed the free vibration and biaxial buckling behaviour of MEE microplate resting on elastic foundation. Based on nonlocal theory Li *et al.* (2016) obtained the bending, buckling and free vibration characteristics of MEE nano beams. Lang and Xuewu (2013) analysed the buckling and vibration characteristics of functionally graded magneto-electro-thermo-elastic circular cylindrical shells. Frajpour and Rastgoo (2017) developed a modified shell model to analyse the buckling behavior of smart composite nanotubes under magneto-electro-mechanical loads. Ebrahimi and Barati (2016b) employed the refined sinusoidal plate model to study the thermo-mechanical buckling problem of magneto-electro-thermo-elastic functionally graded (METEFG) nanoplates supported by Winkler-Pasternak elastic foundation. Razavi (2017) presented the buckling behaviour of smart plates accounting the effect of electric and magnetic potentials using higher order theory. Ebrahimi and Barati (2016c) developed a size-dependent beam model to predict the
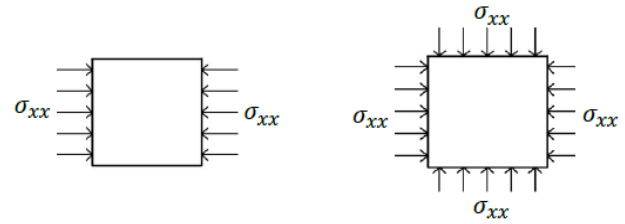
buckling behaviour of MEE nano beams. Ebrahimi and Barti (2016d) extended their studies on buckling of functionally graded piezoelectric (FGP) nanobeams under the influence of thermo-electro-mechanical loads. Li (2014) investigated the buckling behaviour of MEE plate resting on an elastic foundation and evaluated the effect of electric and magnetic loads affecting it. Ebrahimi and Barati (2016e) analysed the static stability of piezoelectrically actuated size-dependent magneto-electro-elastic functionally graded nanoplate.

The comprehensive literature review suggests that extensive research pertaining to free vibration, static studies, nonlinear behaviour, dynamic characteristics of layered and functionally graded MEE plates, beams and shells has been published. In addition, studies concerned with buckling behaviour of functionally graded single layer MEE plates resting on an elastic foundation are recently reported. However, to the authors' best knowledge present work makes a first attempt to analyse the buckling behaviour of multilayerd MEE plates with the aid of FE methods. Consequently, this article presents a finite element model based on FSDT to assess the buckling characteristics of the multilayered MEE plate. The in-plane stress distribution within the MEE plate existing due to the enacted force is considered to be equivalent to the applied in-plane compressive loads in the pre-buckling range. The potential energy functional is formulated based on the same stress distribution. Buckling characteristics are well presented in terms of non-dimensional critical buckling load and their corresponding mode shapes which are obtained by solving a linear eigenvalue problem. In addition, parametric studies such as the effect of uniaxial and biaxial compression, aspect ratio, span to thickness ratio and boundary conditions are studied in detail. Further, the static deflection of MEE plate under different boundary and loading conditions are also presented.

2. Problem description and governing equation

A schematic diagram of a three layered magneto-electro-elastic plate is illustrated in Fig. 1 while Fig. 2 illustrates the two-dimensional *x-y* plane of the MEE plate subjected to uniaxial and biaxial compression.

The length, the width and the total thickness of the plate are *a*, *b* and *H*, respectively. The MEE plate consists of three layers of equal thickness h_i (*i*=1, 2, 3). The top and the bottom layers are made of identical material either piezoelectric (BaTiO$_3$) commonly represented by *B* or

magnetostrictive ($CoFe_2O_4$) commonly represented by *F* while the middle layer is of the other material i.e., magnetostrictive or piezoelectric. Based on the stacking sequence of the material, the MEE composite is called B/F/B or F/B/F indicating the top/middle/bottom layer, respectively, wherein, *B* represents barium titanate and *F* represents cobalt ferrite. The displacement field of such MEE plate is considered as a first order expansion of Taylor's series of the mid-plane variables with respect to the plate thickness. Hence, the displacement fields are given by (Reddy 2004)

$$u = u_0 + z\theta_x , \quad v = v_0 + z\theta_y , \quad w = w_0 \qquad (1)$$

where, u_0, v_0, w_0 are the initial displacements at the midplane and θ_x, θ_y are the rotations of the line initially normal to the midplane relative to the *y*- and *x*- axis respectively. For the ease of computation, the displacement components are split into translational and rotational displacement vectors as follows

$$\{d_t\} = [u_0 \ v_0 \ w_0]^T \quad \{d_r\} = [\theta_x \ \theta_y]^T \qquad (2)$$

Since thin plate analysis is involved, to avoid shear locking selective integration scheme is employed. In addition, to emphasize the effect of transverse shear deformation, the strain (ε) at any point in the MEE plate is divided into bending strain (ε_b) vector and shear strain (ε_s) vector and are written as follows

$$\{\varepsilon\} = \{\varepsilon_x \ \ \varepsilon_y \ \ \varepsilon_z \ \ \varepsilon_{xy} \ \ \varepsilon_{xz} \ \ \varepsilon_{yz}\}^T ,$$
$$\{\varepsilon_b\} = \{\varepsilon_x \ \varepsilon_y \ \varepsilon_z \ \varepsilon_{xy}\}^T , \quad \{\varepsilon_s\} = [\varepsilon_{xz} \ \varepsilon_{yz}]^T \qquad (3)$$

Utilizing the displacement field from Eq. (1) and the strain components in Eq. (3) along with the strain-displacement relations, the state of in-plane, transverse normal and transverse shear stress components at any point in the plate can be expressed as

$$\{\varepsilon_b\} = \{\varepsilon_{bt}\} + [Z_1]\{\varepsilon_{br}\} , \quad \{\varepsilon_s\} = \{\varepsilon_{st}\} + [Z_2]\{\varepsilon_{sr}\} \qquad (4)$$

in which, $[Z_1]$ and $[Z_2]$ are the transformation matrices given as

$$[Z_1] = \begin{bmatrix} z & 0 & 0 \\ 0 & z & 0 \\ 0 & 0 & 0 \\ 0 & 0 & z \end{bmatrix}, \quad [Z_2] = \begin{bmatrix} 1 & 0 \\ 0 & 1 \end{bmatrix} \qquad (5)$$

correspondingly, the various strain components appearing in Eq. (4) are given by

$$\{\varepsilon_{bt}\} = \begin{bmatrix} \dfrac{\partial u_0}{\partial x} & \dfrac{\partial v_0}{\partial y} & 0 & \dfrac{\partial u_0}{\partial y} + \dfrac{\partial v_0}{\partial x} \end{bmatrix}, \ \{\varepsilon_{ts}\} = \begin{bmatrix} \dfrac{\partial w_0}{\partial x} & \dfrac{\partial w_0}{\partial y} \end{bmatrix}$$
$$\{\varepsilon_{br}\} = \begin{bmatrix} \dfrac{\partial \theta_x}{\partial x} & \dfrac{\partial \theta_y}{\partial y} & 0 & \dfrac{\partial \theta_x}{\partial y} + \dfrac{\partial \theta_y}{\partial x} \end{bmatrix} \qquad (6)$$

Analogous to the strain vectors presented in Eq. (3), the stress state at any given point in the MEE plate can be expressed as follows

$$\{\sigma_b\} = \begin{bmatrix} \sigma_x & \sigma_y & \sigma_z & \sigma_{xy} \end{bmatrix}^T , \ \{\sigma_s\} = [\sigma_{xz} \ \sigma_{yz}]^T \qquad (7)$$

wherein, σ_x, σ_y and σ_z along the *x*-, *y*- and *z*-directions are the corresponding normal stresses; the in-plane stress component is σ_{xy}; σ_{xz} and σ_{yz} are the transverse shear stresses along *xz*- and *yz*- directions, respectively. Considering the effect of coupled fields, the constitutive equations for the MEE plate can be written as follows

$$\{\sigma_b^k\} = [\bar{C}_b^k]\{\varepsilon_b^k\} - \{e_b^k\}E_z - \{q_b^k\}H_z , \quad \{\sigma_s^k\} = [\bar{C}_s^k]\{\varepsilon_s^k\} \quad (8a)$$

$$D_z = \{\bar{e}_b^k\}^T\{\varepsilon_b^k\} + \bar{\xi}_{33}^k E_z + \bar{d}_{33}^k H_z \qquad (8b)$$

$$B_z = \{\bar{q}_b^k\}^T\{\varepsilon_b^k\} + \bar{d}_{33}^k E_z + \bar{\mu}_{33}^k H_z \qquad (8c)$$

here *k*= 1, 2, 3 denotes the layer number initiating from the bottom layer of the MEE plate and

$$[\bar{C}_b^k] = \begin{bmatrix} \bar{C}_{11}^k & \bar{C}_{12}^k & \bar{C}_{13}^k & 0 \\ \bar{C}_{12}^k & \bar{C}_{22}^k & \bar{C}_{23}^k & 0 \\ \bar{C}_{13}^k & \bar{C}_{23}^k & \bar{C}_{33}^k & 0 \\ 0 & 0 & 0 & \bar{C}_{66}^k \end{bmatrix}, \quad [\bar{C}_s^k] = \begin{bmatrix} \bar{C}_{55}^k & \bar{C}_{45}^k \\ \bar{C}_{45}^k & \bar{C}_{44}^k \end{bmatrix} \qquad (9)$$

Where $[\bar{C}_b^k]$ and $[\bar{C}_s^k]$ represent the reduced coefficient matrices, $\bar{\xi}_{33}^k$ is the reduced dielectric constant and $\bar{\mu}_{33}^k$ represent the reduced magnetic permeability coefficient; $\bar{d}_{33}^k$ is the reduced electromagnetic coefficient and are given by (Farajpour *et al.* 2016).

$$\bar{C}_{11}^k = C_{11}^k - \frac{(C_{13}^k)^2}{C_{33}^k} , \quad \bar{C}_{12}^k = C_{12}^k - \frac{(C_{13}^k)^2}{C_{33}^k} , \bar{C}_{13}^k = 0 ,$$

$$\bar{C}_{22}^k = C_{22}^k - \frac{(C_{13}^k)^2}{C_{33}^k} , \quad \bar{C}_{23}^k = 0 , \quad \bar{C}_{33}^k = 0 , \quad \bar{C}_{44}^k = C_{44}^k ,$$

$$\bar{C}_{55}^k = C_{55}^k , \quad \bar{C}_{66}^k = C_{66}^k , \quad \bar{e}_{31}^k = e_{31}^k - \frac{C_{13}^k e_{33}^k}{C_{33}^k} ,$$

$$\bar{e}_{32}^k = e_{32}^k - \frac{C_{13}^k e_{33}^k}{C_{33}^k} , \quad \bar{q}_{31}^k = q_{31}^k - \frac{C_{13}^k q_{33}^k}{C_{33}^k} , \qquad (10)$$

$$\bar{q}_{32}^k = q_{32}^k - \frac{C_{13}^k q_{33}^k}{C_{33}^k}$$

$$\bar{\xi}_{33}^k = \xi_{33}^k - \frac{e_{33}^k q_{33}^k}{C_{33}^k} , \quad \bar{\mu}_{33}^k = \mu_{33}^k - \frac{e_{33}^k q_{33}^k}{C_{33}^k} \quad \text{and}$$

$$\bar{d}_{33}^k = d_{33}^k - \frac{e_{33}^k q_{33}^k}{C_{33}^k}$$

Since the plate is considered to be thin, the electric displacement, the electric field, the magnetic induction and the magnetic field along the *z*-direction are only considered (Milazzo 2014, Sladek *et al.* 2013, Li 2014) and represented by D_z, E_z, B_z and H_z, respectively. The reduced electric coefficient matrix $\{\bar{e}_b^k\}$ and the reduced magnetic coefficient matrix $\{\bar{q}_b^k\}$ are given by

$$\{\bar{e}_b^k\} = \{\bar{e}_{31}^k \ \bar{e}_{32}^k \ \bar{e}_{33}^k \ \bar{e}_{36}^k\}^T , \quad \{\bar{q}_b^k\} = \{\bar{q}_{31}^k \ \bar{q}_{32}^k \ \bar{q}_{33}^k \ \bar{q}_{36}^k\}^T \qquad (11)$$

Employing the principle of virtual work the governing equations for the MEE plate is established as

$$\delta \prod = \delta U + \delta V = 0 \qquad (12)$$

wherein, the strain energy (δU) is given by

$$\delta U = \sum_{k=I}^{3} \left(\int_{\Lambda^k} \delta \{\varepsilon_b^k\}\{\sigma_b^k\} d\Lambda^k + \int_{\Lambda^k} \delta \{\varepsilon_s^k\}\{\sigma_s^k\} d\Lambda^k \right)$$
$$- \int_{\Lambda^t} \delta E_z^t\, D_z^t d\Lambda^t - \int_{\Lambda^b} \delta E_z^b\, D_z^b d\Lambda^b \qquad (13)$$
$$- \int_{\Lambda^m} \delta H_z\, B_z d\Lambda^m - \int_{A^{el}} \delta \{d_t\}^T\, F_t\ dA^{el}$$

and simultaneously the work of in-plane loads (δV) can be expressed as

$$\delta V = \int_0^a \int_0^b \begin{bmatrix} \dfrac{\partial w}{\partial x} \\ \dfrac{\partial w}{\partial y} \end{bmatrix}^T [\sigma_0] \begin{bmatrix} \dfrac{\partial w}{\partial x} \\ \dfrac{\partial w}{\partial y} \end{bmatrix} dx\, dy \qquad (14)$$

where Λ^k (k=1, 2, 3) designates the respective layer volume, F_i corresponds to the applied surface traction force on the top surface area A^{el}. Λ^t and Λ^b represent the volume of the top and bottom piezoelectric while the middle magnetostrictive layer is represented by Λ^m. $[\sigma_0]$ is the initial stress matrix. E_z^t, E_z^b and D_z^t, D_z^b are the electric fields and the electric displacements of the top and the bottom layers of the MEE plate whereas H_z^m and B_z^m are the magnetic field and magnetic induction in the middle layer, respectively. The transverse electric field (E_z) related to the electric potential and the transverse magnetic field (H_z) is related to the magnetic potential in accordance with Maxwell's equation as follows

$$E_z^t = -\frac{\partial \phi^t}{\partial z}, \quad E_z^b = -\frac{\partial \phi^b}{\partial z} \quad \text{and} \quad H_z^m = -\frac{\partial \psi^m}{\partial z} \qquad (15)$$

where, *t/b/m* represent the top/bottom/middle layer of the MEE plate, respectively, depending on the stacking sequence of the layers. The interface linking piezoelectric and magnetostrictive layers are assumed to be properly grounded. Since the MEE plate layers possess very small thickness, the variation of the electric and magnetic potential across the thickness can be suitably assumed to be linear. Correspondingly, the electric potential functions ϕ^t and ϕ^b pertaining to the top and bottom piezoelectric layers and ψ^m the magnetic potential pertaining to the middle magnetostrictive layer of the MEE plate (Kattimani 2015) can be represented as

$$\phi^t = \frac{z - z_b}{h} \phi_1, \quad \phi^b = -\frac{z - h_2}{h} \phi_2 \quad \text{and} \quad \psi^m = \frac{z - h_2}{h} \bar{\psi} \qquad (16)$$

2.1 Finite element formulation

The MEE plate is discretized by using four noded quadrilateral elements. Considering Eq. (2), the displacement vectors in generalized form $\{d_u\}$ and $\{d_n\}$ are linked with the ith node (where, i = 1, 2, 3, 4) of an element can be articulated as

$$\{d_{ti}\} = [u_{0i}\ v_{0i}\ w_{0i}]^T \quad \text{and} \quad \{d_{ri}\} = [\theta_{xi}\ \theta_{yi}]^T \qquad (17)$$

At any given point within the element, the displacement vectors in generalized form $\{d_t\}$ and $\{d_r\}$, the generalized electric potential vector $\{\phi\}$ and the generalized magnetic potential vector $\{\psi\}$ can be expressed in terms of nodal generalized displacement vectors $\{d_t^{el}\}$ and $\{d_r^{el}\}$, the nodal magnetic potential vector $\{\psi^{el}\}$ and the nodal electric potential vector $\{\phi^{el}\}$, respectively, as follows

$$\{d_t\} = [n_t]\{d_t^{el}\}, \quad \{d_r\} = [n_r]\{d_r^{el}\},$$
$$\{\phi\} = [\phi_1\ \phi_2]^T = [n_\phi]\{\phi^{el}\} \quad , \qquad (18)$$
$$\{\psi\} = [\psi_1\ \psi_2]^T = [n_\psi]\{\psi^{el}\} \quad \text{and} \quad \{\psi^m\} = [n_\psi^m]\{\psi_m^{el}\}$$

in which

$$\{d_t^{el}\} = \left[\{d_{t1}^{el}\}^T\ \{d_{t2}^{el}\}^T \cdots \{d_{t4}^{el}\}^T \right]^T ,$$
$$\{d_r^{el}\} = \left[\{d_{r1}^{el}\}^T\ \{d_{r2}^{el}\}^T \cdots \{d_{r4}^{el}\}^T \right]^T ,$$
$$\{\phi^{el}\} = \{\phi_{11}\ \phi_{21}\ \phi_{12}\ \phi_{22} \cdots \phi_{14}\ \phi_{24}\}^T ,$$
$$\{\bar{\psi}^{el}\} = \{\bar{\psi}_1\ \bar{\psi}_2 \cdots \bar{\psi}_4\}^T ,$$
$$[n_t] = [n_{t1}\ n_{t2} \cdots n_{t4}]^T, \quad [n_r] = [n_{r1}\ n_{r2} \cdots n_{r4}]^T, \qquad (19)$$
$$[n_\phi] = \begin{bmatrix} n_{\phi 1} & 0 & n_{\phi 2} & 0 & \cdots & n_{\phi 4} & 0 \\ 0 & n_{\phi 21} & 0 & n_{\phi 22} & \cdots & 0 & n_{\phi 24} \end{bmatrix}^T ,$$
$$[n_\psi] = [n_{\psi 1}\ n_{\psi 2} \cdots n_{\psi 4}]^T ,$$
$$n_{ti} = N_i I_t, \quad n_{ri} = N_i I_r$$

where $[n_i]$, $[n_r]$, $[n_\phi]$ and $[n_\psi]$ are the shape function matrices while I_t and I_r are the identity matrices, respectively (Kattimani 2015). The shape function N_i corresponding to the natural coordinate is linked with the ith node. The degrees of freedom corresponding to electric potential and magnetic potential are ϕ_{1i}, ϕ_{2i} (where, i=1, 2, 3, 4) and $\bar{\psi}_i$, respectively. Utilizing Eqs. (13)-(17), the transverse electric field for the top and the bottom layer (E_z^t, E_z^b) and the transverse magnetic field for the middle layer (H_z^m) are given by

$$E_z^t = -\frac{1}{h}[1\ \ 0][n_\phi]\{\phi^{el}\},$$
$$\qquad (20)$$
$$E_z^b = -\frac{1}{h}[0\ \ 1][n_\phi]\{\phi^{el}\} \quad \text{and} \quad H_z^m = -\frac{1}{h}[n_\psi]\{\psi^{el}\}$$

Now, considering Eqs. (4) and (17), the strain vectors in generalized form at any given point in the element can be presented in the form of nodal generalized strain vectors as

$$\{\varepsilon_{bt}\} = [b_{bt}]\{d_t^{el}\} \quad , \quad \{\varepsilon_{br}\} = [b_{br}]\{d_r^{el}\}$$
$$\{\varepsilon_{st}\} = [b_{st}]\{d_t^{el}\} \quad , \quad \{\varepsilon_{sr}\} = [b_{sr}]\{d_r^{el}\} \qquad (21)$$

in which, $[b_{tb}]$, $[b_{rb}]$, $[b_{ts}]$ and $[b_{rs}]$ are the nodal strain-displacement matrices. The explicit form of the matrices is given in the appendix. Substituting Eqs. (4), (11), (14), (20) and (21) into Eq. (12) and simplifying, we obtain the elemental equations of motion for the MEE plate as follows

$$\begin{aligned} &\left[k_{tt}^{el}\right]\left\{d_t^{el}\right\}+\left[k_{tr}^{el}\right]\left\{d_r^{el}\right\}+\left[k_{t\phi}^{el}\right]\left\{\phi^{el}\right\}+\left[k_{t\psi}^{el}\right]\left\{\psi^{el}\right\} \\ &+\left[k_G^{el}\right]\left\{d_t\right\}=\left\{F_t^{el}\right\} \end{aligned} \quad (22)$$

$$\left[k_{tr}^{el}\right]^{\mathrm{T}}\left\{d_t^{el}\right\}+\left[k_{rr}^{el}\right]\left\{d_r^{el}\right\}+\left[k_{r\phi}^{el}\right]\left\{\phi^{el}\right\}+\left[k_{r\psi}^{el}\right]\left\{\psi^{el}\right\}=0 \quad (23)$$

$$\left[k_{t\phi}^{el}\right]^{\mathrm{T}}\left\{d_t^{el}\right\}+\left[k_{r\phi}^{el}\right]^{\mathrm{T}}\left\{d_r^{el}\right\}-\left[k_{\phi\phi}^{el}\right]\left\{\phi^{el}\right\}=0 \quad (24)$$

$$\left[k_{t\psi}^{el}\right]^{\mathrm{T}}\left\{d_t^{el}\right\}+\left[k_{r\psi}^{el}\right]^{\mathrm{T}}\left\{d_r^{el}\right\}-\left[k_{\psi\psi}^{el}\right]\left\{\psi^{el}\right\}=0 \quad (25)$$

The matrices and the vectors displayed in the Eqs. (22)-(25) are the elemental elastic stiffness matrices $\left[k_{tt}^{el}\right]$, $\left[k_{tr}^{el}\right]$ and $\left[k_{rr}^{el}\right]$, the elemental electro-elastic coupling stiffness and magneto-elastic coupling stiffness matrices are $\left[k_{t\phi}^{el}\right]$, $\left[k_{r\phi}^{el}\right]$ and $\left[k_{t\psi}^{el}\right]$, $\left[k_{r\psi}^{el}\right]$, respectively; $\left[k_G^{el}\right]$ is the elemental geometric stiffness matrix; $\left\{F_t^{el}\right\}$ is the elemental mechanical load vector; $\left[k_{\phi\phi}^{el}\right]$ and $\left[k_{\psi\psi}^{el}\right]$ are the elemental electric and elemental magnetic stiffness matrices, respectively. The elemental matrices and vectors are given by

$$\left[k_{tt}^{el}\right]=\left[k_{tb}^{el}\right]+\left[k_{ts}^{el}\right], \quad \left[k_{tr}^{el}\right]=\left[k_{trb}^{el}\right]+\left[k_{trs}^{el}\right],$$

$$\left[k_{rr}^{el}\right]=\left[k_{rrb}^{el}\right]+\left[k_{rrs}^{el}\right], \quad \left[k_{t\phi}^{el}\right]=\left[k_{\phi t}^{el}\right]^T,$$

$$\left[k_{t\psi}^{el}\right]=\left[k_{\psi t}^{el}\right]^T, \quad \left[k_{t\phi}^{el}\right]=\int_0^{a_{el}}\int_0^{b_{el}}\left[b_{tb}\right]^T\left[D_{t\phi}\right]\left[n_\phi\right]dx\,dy,$$

$$\left[k_{r\phi}^{el}\right]=\int_0^{a_{el}}\int_0^{b_{el}}\left[b_{rb}\right]^T\left[D_{r\phi}\right]\left[n_\phi\right]dx\,dy,$$

$$\left[k_{t\psi}^{el}\right]=\int_0^{a_{el}}\int_0^{b_{el}}\left[b_{tb}\right]^T\left[D_{t\psi}\right]\left[n_\psi\right]dx\,dy,$$

$$\left[k_{r\psi}^{el}\right]=\int_0^{a_{el}}\int_0^{b_{el}}\left[b_{rb}\right]^T\left[D_{r\psi}\right]\left[n_\psi\right]dx\,dy,$$

$$\left[k_{\phi\phi}^{el}\right]=\int_0^{a_{el}}\int_0^{b_{el}}\left[n_\phi\right]^T\left[D_{\phi\phi}\right]\left[n_\phi\right]dx\,dy,$$

$$\left[k_{\psi\psi}^{el}\right]=\int_0^{a_{el}}\int_0^{b_{el}}\left[n_\psi\right]^T\left[D_{\psi\psi}\right]\left[n_\psi\right]dx\,dy,$$

$$\left[k_G^{el}\right]=\int_0^{a_{el}}\int_0^{b_{el}}\left[b_G\right]^T\left[\sigma_0\right]\left[b_G\right]dx\,dy$$

$$(26)$$

where, $[D_{t\phi}]$, $[D_{r\phi}]$, $[D_{t\psi}]$, $[D_{r\psi}]$, $[D_{\phi\phi}]$ and $[D_{\psi\psi}]$ are the rigidity matrices appearing in Eq.(26) are given as follows

$$\left[D_{t\phi}\right]=\int_{h_3}^{h_4}\{e_b\}\frac{1}{h}\begin{bmatrix}1 & 0\end{bmatrix}dz+\int_{h_1}^{h_2}\{e_b\}\frac{1}{h}\begin{bmatrix}1 & 0\end{bmatrix}dz,$$

$$\left[D_{t\psi}\right]=\int_{h_2}^{h_3}\{q_b\}\frac{1}{h}\,dz,$$

$$\left[D_{r\phi}\right]=\int_{h_3}^{h_4}[z_1]^T\{e_b\}\frac{1}{h}\begin{bmatrix}1 & 0\end{bmatrix}dz+\int_{h_1}^{h_2}[z_1]^T\{e_b\}\frac{1}{h}\begin{bmatrix}1 & 0\end{bmatrix}dz,$$

$$\left[D_{r\psi}\right]=\int_{h_2}^{h_3}[z_1]^T\{q_b\}\frac{1}{h}dz, \quad (27)$$

$$\left[D_{\phi\phi}\right]=\frac{\xi_{33}}{h}\begin{bmatrix}1 & 0\\0 & 1\end{bmatrix}, \quad D_{\psi\psi}=\frac{1}{h}\mu_{33}, \quad [\sigma_0]=\begin{bmatrix}\sigma_{xx}^0 & \sigma_{xy}^0\\\sigma_{xy}^0 & \sigma_{yy}^0\end{bmatrix}$$

The global equations of motion are obtained assembling the elemental equations of motion of the MEE plate as follows

$$\begin{aligned} &\left[k_{tt}^g\right]\{d_t\}+\left[k_{tr}^g\right]\{d_r\}+\left[k_{t\phi}^g\right]\{\phi\}+\left[k_{t\psi}^g\right]\{\psi\} \\ &+\left[K_G\right]\{d_t\}=\{F_t\} \end{aligned} \quad (28)$$

$$\left[k_{tr}^g\right]^{\mathrm{T}}\{d_t\}+\left[k_{rr}^g\right]\{d_r\}+\left[k_{r\phi}^g\right]\{\phi\}+\left[k_{r\psi}^g\right]\{\psi\}=0 \quad (29)$$

$$\left[k_{t\phi}^g\right]^{\mathrm{T}}\{d_t\}+\left[k_{r\phi}^g\right]^{\mathrm{T}}\{d_r\}-\left[k_{\phi\phi}^g\right]\{\phi\}=0 \quad (30)$$

$$\left[k_{t\psi}^g\right]^{\mathrm{T}}\{d_t\}+\left[k_{r\psi}^g\right]^{\mathrm{T}}\{d_r\}-\left[k_{\psi\psi}^g\right]\{\psi\}=0 \quad (31)$$

where, $\left[k_{tt}^g\right]$, $\left[k_{tr}^g\right]$ and $\left[k_{rr}^g\right]$ are the elastic global stiffness matrices; $\left[k_{t\phi}^g\right]$ and $\left[k_{r\phi}^g\right]$ are the electro-elastic coupling global stiffness matrices; $\left[k_{t\psi}^g\right]$ and $\left[k_{r\psi}^g\right]$ are the magneto-elastic coupling global stiffness matrices; $[K_G]$ is the global geometric stiffness matrix; $\{F_t\}$ is the global mechanical load vector; $\left[k_{\phi\phi}^g\right]$ and $\left[k_{\psi\psi}^g\right]$ are the global electric and the global magnetic stiffness matrices, respectively. Solving the global equations of motion (Eqs. (29)-(31)) to obtain the global generalized displacement vector $\{d_t\}$ and $\{d_r\}$ by condensing the global degrees of freedom for $\{\phi\}$ and $\{\psi\}$ in terms of $\{d_r\}$ as follows

$$\{\psi\}=\left[k_{\psi\psi}^g\right]^{-1}\left[k_{t\psi}^g\right]^{\mathrm{T}}\{d_t\}+\left[k_{\psi\psi}^g\right]^{-1}\left[k_{r\psi}^g\right]^{\mathrm{T}}\{d_r\},$$

$$\{\phi\}=\left[k_{\phi\phi}^g\right]^{-1}\left[k_{t\phi}^g\right]^{\mathrm{T}}\{d_t\}+\left[k_{\phi\phi}^g\right]^{-1}\left[k_{r\phi}^g\right]^{\mathrm{T}}\{d_r\}, \quad (32)$$

$$\{d_r\}=-\left[K_3\right]^{-1}\left[K_2\right]^{\mathrm{T}}\{d_t\}$$

Now, substituting Eq. (32) in Eq. (28) and upon simplification, we obtain the global equations of motion in terms of the global translational degrees of freedom as follows

$$\left(\left[K_1\right]-\left[K_2\right]\left[K_3\right]^{-1}\left[K_2\right]^{\mathrm{T}}\right)\{d_t\}+\left[K_G\right]\{d_t\}=\{F_t\},$$

$$[K]\{d_t\}+\left[K_G\right]\{d_t\}=\{F_t\} \quad (33)$$

$$\text{and } [K]=\left(\left[K_1\right]-\left[K_2\right]\left[K_3\right]^{-1}\left[K_2\right]^{\mathrm{T}}\right)$$

where, the global aggrandized matrices are given as follows

$$\left[K_1\right]=\left[k_{tt}^g\right]+\left[k_{t\phi}^g\right]\left[k_{\phi\phi}^g\right]^{-1}\left[k_{t\phi}^g\right]^{\mathrm{T}}+\left[k_{t\psi}^g\right]\left[k_{\psi\psi}^g\right]^{-1}\left[k_{t\psi}^g\right]^{\mathrm{T}},$$

$$\left[K_2\right]=\left[k_{tr}^g\right]+\left[k_{t\phi}^g\right]\left[k_{\phi\phi}^g\right]^{-1}\left[k_{r\phi}^g\right]^{\mathrm{T}}+\left[k_{t\psi}^g\right]\left[k_{\psi\psi}^g\right]^{-1}\left[k_{r\psi}^g\right]^{\mathrm{T}}, \quad (34)$$

$$\left[K_3\right]=\left[k_{rr}^g\right]+\left[k_{r\phi}^g\right]\left[k_{\phi\phi}^g\right]^{-1}\left[k_{r\phi}^g\right]^{\mathrm{T}}+\left[k_{r\psi}^g\right]\left[k_{\psi\psi}^g\right]^{-1}\left[k_{r\psi}^g\right]^{\mathrm{T}}$$

The buckling criterion is achieved based on neutral

Table 1 Material properties of BaTiO$_3$ and CoFe$_2$O$_4$ (Pan and Heyliger 2003)

Material	$C_{11} = C_{22}$ (10^9 N/m^2)	C_{12} (10^9 N/m^2)	$C_{13}=C_{23}$ (10^9 N/m^2)	C_{33} (10^9 N/m^2)	$C_{44}=C_{55}$ (10^9 N/m^2)	C_{66} (10^9 N/m^2)	ρ (kg/m^3)
BaTiO$_3$	166	77	78	162	43	44.5	5800
CoFe$_2$O$_4$	286	173	170.5	269.5	45.3	56.5	5300
BaTiO$_3$	$e_{31}=e_{32}=-4.4$ (C/m^2)	$e_{33}=18.6$ (C/m^2)	$e_{24}=e_{15}=11.6$ (C/m^2)	$\xi_{11}=\xi_{22}=11.2$ (10^{-9} C/Nm^2)	ξ_{33}(10^{-9} C/Nm^2) =12.6	$\mu_{11}=\mu_{22}=5$ (10^{-6} Ns^2/C^2)	$\mu_{33}=10$ (10^{-6} Ns^2/C^2)
CoFe$_2$O$_4$	$q_{31}=q_{32}$ (N/Am) =180.3	q_{33} (N/Am) = 699.7	$q_{24}=q_{15}=550$ (N/Am)	$\xi_{11}=\xi_{22}=0.08$ (10^{-9} C/Nm^2)	$\xi_{33}=0.093$ (10^{-9} C/Nm^2)	$\mu_{11}=\mu_{22}=-590$ (10^{-6} Ns^2/C^2)	$\mu_{33}=157$ (10^{-6} Ns^2/C^2)

equilibrium method (Jadhav and Bajoria 2013). According to this method, the corresponding load at which the structure attains equilibrium in both straight and the slightly bent configuration is defined as a critical load. The geometric matrix is represented by $\lambda[K_G]$, where λ is the scalar multiplier. The scalar multiplier is obtained such that, the equilibrium is established for both the reference configuration $\{d_t\}$ and slightly deformed configuration $\{d_t\}+\{\delta d_t\}$ (Jadhav and Bajoria 2013).

$$\left([K]+\lambda[K_G]\right)\{d_t\}=\{F_t\} \quad (35)$$

$$\left([K]+\lambda[K_G]\right)\left(\{d_t\}+\{\delta d_t\}\right)=\{F_t\} \quad (36)$$

Subtracting Eq. (36) from Eq. (35) yields the eigenvalue problem

$$\left([K]+\lambda[K_G]\right)\{\delta d_t\}=0 \quad (37)$$

here, the critical buckling load is the eigenvalue with the lowest magnitude and the displacement vector $\{\delta d_t\}$ represents the corresponding buckled mode shape. Further, the static behaviour of the MEE plate is assessed by neglecting the geometrical stiffness matrix from Eq. (35).

3. Results and discussion

3.1 Buckling analysis

Buckling analysis of layered magneto-electro-elastic plate is carried out in order to assess the nature of stability by building an eigenvalue problem. Such eigenvalue problem yields eigen values i.e., critical buckling loads and their corresponding mode shapes in terms of eigen vectors. The multilayered MEE plate involved in this study is made of piezoelectric (BaTiO$_3$) and magnetostrictive (CoFe$_2$O$_4$) material both being transversely isotropic. The material property of the MEE composite is specified in Table 1. Two types of stacking sequence are studied one being B/F/B i.e., the magnetostrictive layer being sandwiched between two piezoelectric layers and the other being F/B/F wherein the piezoelectric layer is sandwiched between two magnetostrictive layers. The buckling characteristics of the MEE plate is evaluated for different aspect ratio, span to thickness ratio and boundary condition. In addition, the effect of load factor on the critical buckling load is subsequently investigated. The MEE plate considered for the analysis is having an aspect ratio of $a/b=1$ m and a span to thickness ratio of $a/h=100$ with each layer having equal

thickness. The non-dimensional critical buckling load is obtained using $\lambda_{cr}=\lambda a^2/H^3 C^{11}$. In the present study, buckling analysis is performed for three boundary conditions i.e., CCCC (all sides clamped), CCCF (three clamped sides and one being free), FCFC (two clamped and two free sides) which are given as (Ansari and Gholami 2016)

Clamped edge
at $x = 0$, $x = a$
$$u_0 = v_0 = w_0 = \theta_x = \theta_y = \theta_z = \phi = \psi = 0$$
at $y = 0$, $y = b$
$$u_0 = v_0 = w_0 = \theta_x = \theta_y = \theta_z = \phi = \psi = 0$$
Free edge
at $x = y$, $x = a$
$$u_0 = v_0 = w_0 = \theta_x = \theta_y = \theta_z = \phi = \psi \neq 0$$
at $y = 0$, $y = b$
$$u_0 = v_0 = w_0 = \theta_x = \theta_y = \theta_z = \phi = \psi \neq 0$$

(38)

3.1.1 Validation

To the best of author's knowledge, research on buckling of layered MEE plate is unavailable in the open literature. Hence, to assess the effectiveness of proposed formulation in solving a stability problem, the buckling analysis of multilayered laminate composites studied by Reddy (2004) has been considered. In this regard, the coupled constitutive equation of the MEE plate has been decoupled and implemented for the analysis of laminated composite plate. The convergence studies has been carried out and for a mesh size of 20×20, the present solutions are well in agreement with existing ones as shown in Table 2 and

Table 2 Non-dimensional critical buckling load for three layered composite plate under uniaxial and biaxial compression

a/h ratio	Type of load	Non-dimensional critical buckling load					
		Present (8×8)	Present (12×12)	Present (16×16)	Present (20×20)	Present (30×30)	Reddy (2004)
10	Uniaxial	15.6930	15.2636	14.9178	14.8690	14.8694	15.2890
	Biaxial	7.8465	7.6318	7.4589	7.4345	7.4347	7.6445
50	Uniaxial	23.2294	22.4276	22.1628	22.0418	22.0422	22.9781
	Biaxial	11.6147	11.2138	11.0814	11.0209	11.0211	11.4890
100	Uniaxial	23.8362	23.0434	22.8826	22.8461	22.8467	23.3633
	Biaxial	11.9181	11.5217	11.4413	11.4230	11.4233	11.6820

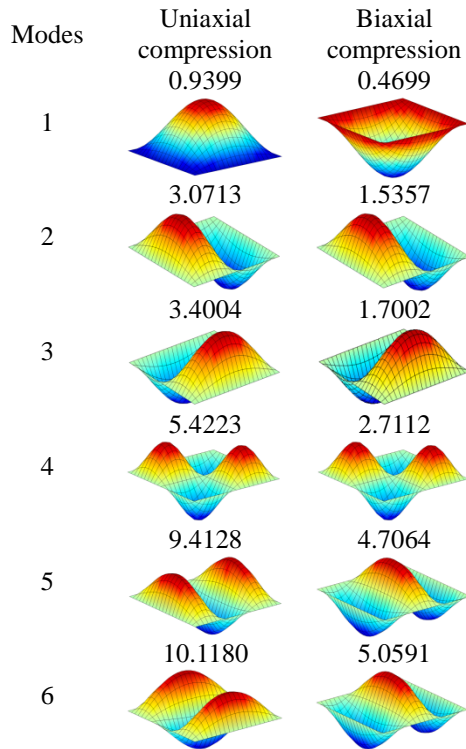| Modes	Uniaxial compression	Biaxial compression
1	0.9399	0.4699
2	3.0713	1.5357
3	3.4004	1.7002
4	5.4223	2.7112
5	9.4128	4.7064
6	10.1180	5.0591

Fig. 3 Comparison of first six buckling mode shapes of B/F/B MEE plate subjected to uniaxial and biaxial compression for CCCC boundary (*a/b*=1, *a/h*=100)
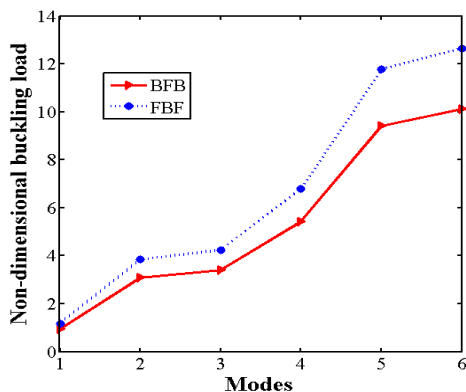
Modes	BFB	FBF
1	0.9399	1.1750
2	3.0713	3.8392
3	3.4004	4.2505
4	5.4223	6.7779
5	9.4128	11.7660
6	10.1180	12.6477

Fig. 5 Comparison of first six non-dimensional critical buckling loads and mode shapes of B/F/B and F/B/F plate subjected to uniaxial compression under clamped-clamped (CCCC) boundary condition (*a/b*=1, *a/h*=100)

Fig. 4 Critical buckling load for B/F/B and F/B/F MEE plate subjected to uniaxial compression. (CCCC, *a/b*=1, *a/h*=100)

apparently for all the subsequent analysis, a mesh size of 20×20 (400 elements) has been imparted.

3.1.2 Effect of uniaxial and biaxial compression

Firstly, buckling analysis of clamped-clamped MEE plates subjected to uniaxial and biaxial compression is investigated. Consequently, their influence on the non-dimensional critical buckling load and their corresponding mode shapes are analysed. The MEE plate having an aspect ratio of *a/b* = 1 and a span to thickness ratio of *a/h* = 100 is considered for the analysis. Buckling mode shapes and their respective buckling loads are presented in Fig. 3. It can be observed that the buckling loads get halved for the bi-axial load in comparison with uniaxial loading case. It is also

evident from the results that the first, fifth and sixth modes of the MEE plate under biaxial compression buckled in the opposite direction in comparison with uniaxial compression; while, the nature of the buckling mode remained the same in both the cases.

3.1.3 Effect of stacking sequence

In this section, the effect of stacking sequence on the buckling behaviour of MEE plates is considered for evaluation. Two stacking sequences of MEE plate are investigated under clamped-clamped boundary condition. Fig. 4 display the buckling behaviour of the B/F/B and the F/B/F stacking pattern. It can be observed from the plots that the MEE plate with F/B/F stacking yield higher critical buckling load than the B/F/B stacking configuration. It may be due to the fact that the F/B/F configuration exhibit higher stiffness and hence larger buckling load. Fig. 5 illustrates the first six non-dimensional critical buckling loads and their corresponding mode shapes for both the B/F/B and F/B/F stacking sequences of the MEE plate. It may be observed from these results that the stacking sequence not only affects the critical buckling loads but also their corresponding mode shapes. In addition as noticed from Fig. 5, the first, third, fifth and sixth modes display buckling in opposite direction for F/B/F sequence in comparison with B/F/B stacking while the nature of buckling remains the same for both.

3.1.4 Effect of lateral load parameter

In a bi-axial buckling condition, the lateral load on one of the in-plane direction is increased incrementally while in
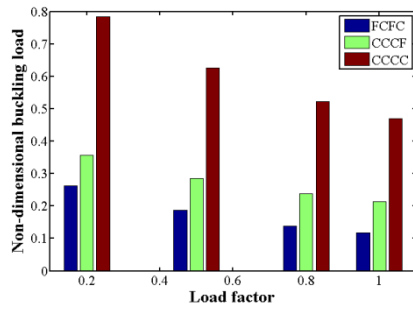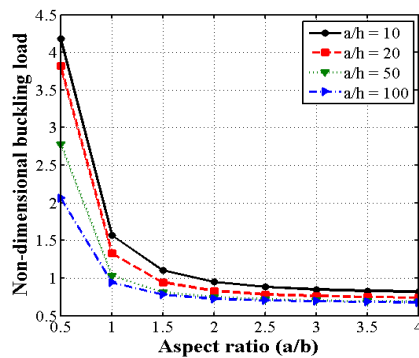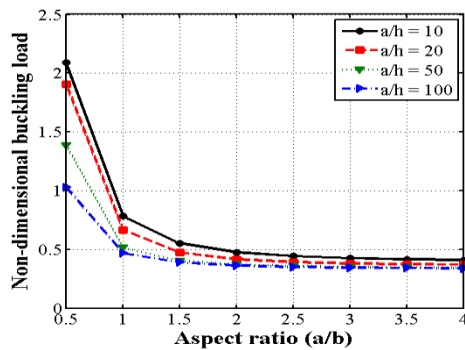
Fig. 6 Effect of load factor on non-dimensional critical buckling load
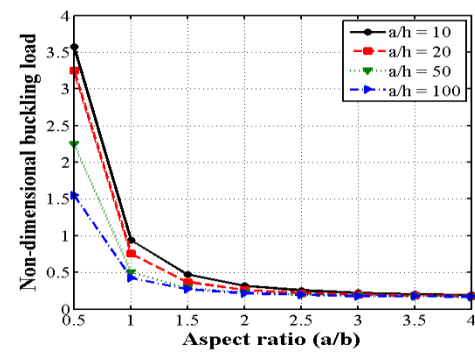

(a) Uniaxial compression

(b) Biaxial compression

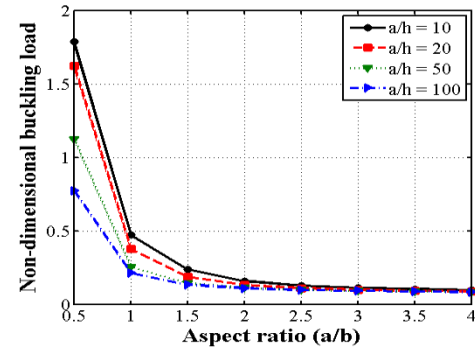Fig. 7 Effect of aspect ratio on Non-dimensional buckling load of MEE (B/F/B) plate under CCCC boundary condition
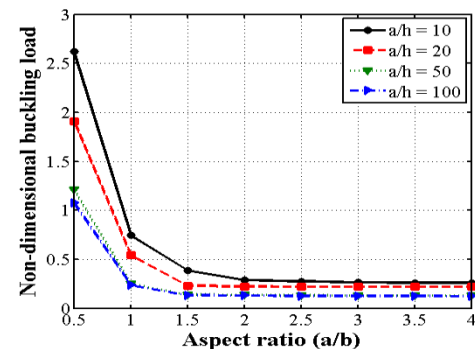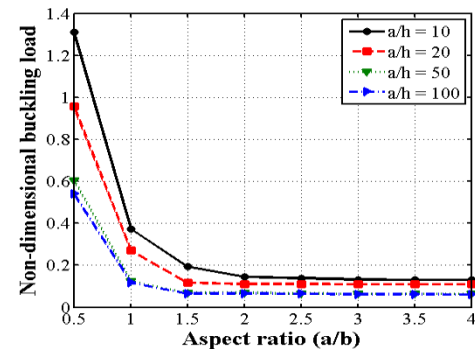

(a) Uniaxial compression

(b) Biaxial compression

Fig. 8 Effect of aspect ratio on Non-dimensional buckling load of MEE (B/F/B) plate under CCCF boundary condition

(a) Uniaxial compression

(b) Biaxial compression

Fig. 9 Effect of aspect ratio on Non-dimensional buckling load of MEE (B/F/B) plate under FCFC boundary condition

the other direction the load is kept constant and their effect on the buckling behaviour of the MEE plate is investigated. The MEE plate subjected to three different boundary conditions (i.e., CCCC, CCCF, and FCFC) is analyzed. A bar graph plotted for buckling load against the load factor in Fig. 6 clearly display a decrease in non-dimensional buckling load with the incremental increase in load factor. It can also be observed that the CCCC boundary condition possess the highest buckling load which can be attributed to the fact that higher the constraint larger is the critical buckling load.

3.1.5 Effect of aspect ratio (a/b)

The buckling characteristic of the MEE plate is studied for different aspect ratios. Non-dimensional critical buckling loads are obtained for different aspect ratio with a particular a/h ratio and the study is extended for four

different span to thickness ratio. Similar results are plotted for different boundary condition as shown in Figs. 7 - 9. It is evident from the plots that the buckling load decreases
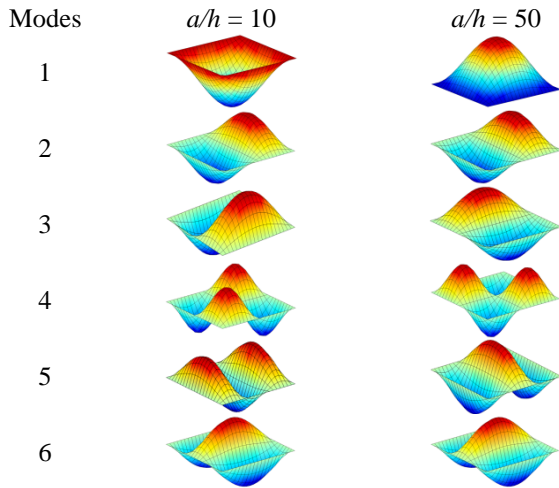
Modes	a/h = 10	a/h = 50
1		
2		
3		
4		
5		
6		

Fig. 10 Comparison of first six non-dimensional buckling mode shapes of B/F/B at *a/h*=10 and 50 subjected to uniaxial compression under clamped-clamped (CCCC) boundary condition

Table 3 Critical buckling loads for B/F/B plate with different span to thickness ratio under uniaxial and biaxial compression

a/h ratio	Uniaxial compression			Biaxial compression		
	CCCC	CCCF	FCFC	CCCC	CCCF	FCFC
20	1.3335	0.7559	0.5405	0.6667	0.3779	0.2702
50	1.0312	0.4317	0.2703	0.5156	0.2158	0.1351
100	0.9399	0.4289	0.2519	0.4699	0.2144	0.1259

with increase in aspect ratio irrespective of the boundary condition and *a/h* ratio involved. The buckling load is observed to decrease rapidly at first and for higher aspect ratios decay is marginal. In the case of CCCF boundary condition, it observed that for all *a/h* ratios evaluated buckling load converges at higher aspect ratios.

3.1.6 Effect of span to thickness (a/h) ratio

The buckling behaviour of clamped-clamped MEE plate is evaluated for different a/h ratios to analyse their effect on buckling loads. Table 3 presents the critical buckling loads obtained for the different span to thickness ratio (*a/h*=20, 50 and 100) of the MEE plate under uniaxial and biaxial loading conditions. It is observed that with the increase in thickness ratio, the critical buckling load decreases for both the uniaxial and biaxial compression. The effect of the span to thickness ratio on the corresponding mode shapes is also presented in Fig. 10. From the results, it is evident that the mode shapes and their corresponding critical buckling loads are influenced by the span to thickness ratio of the plate. Further, it can be observed that the nature of the modes remains the same for both the *a/h* ratio compared; while for the first, third, fourth and fifth modes only the direction of buckling changes. It can be noted that for an eigen buckling problem, the direction of mode shape distribution retains less importance and the very nature of buckling mode shape for both the span to thickness ratio can be considered identical. The same is also true for the case of stacking sequence.
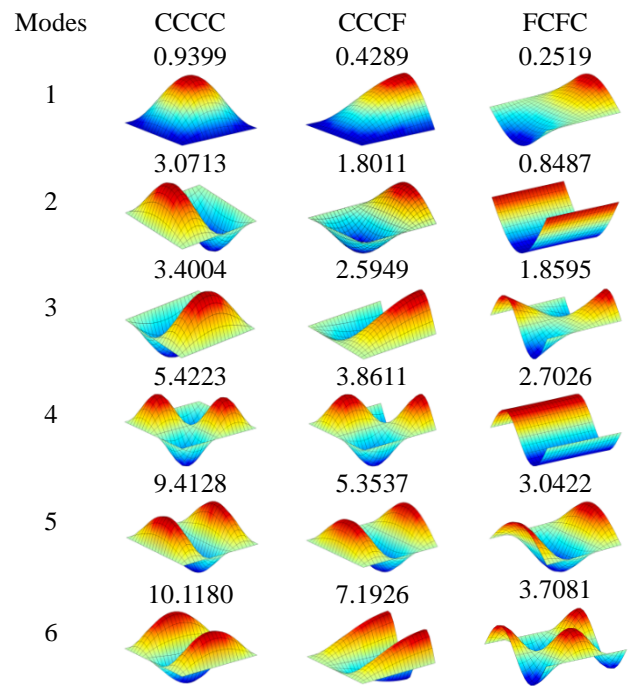
Modes	CCCC	CCCF	FCFC
1	0.9399	0.4289	0.2519
2	3.0713	1.8011	0.8487
3	3.4004	2.5949	1.8595
4	5.4223	3.8611	2.7026
5	9.4128	5.3537	3.0422
6	10.1180	7.1926	3.7081

Fig. 11 Comparison of first six non-dimensional buckling loads and their mode shapes for different boundary condition of B/F/B MEE plate (*a/b*=1, *a/h*=100)
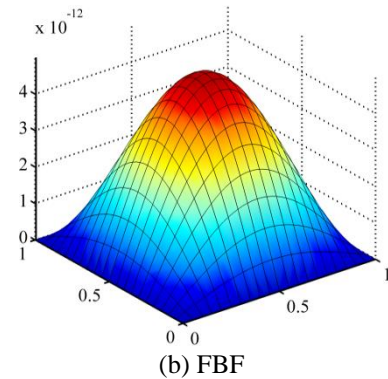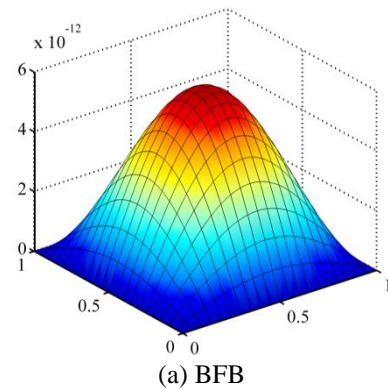

(a) BFB

(b) FBF

Fig. 12 Static deflection (in meters) of simply supported MEE plate subjected to sinusoidal load

3.1.7 Effect of boundary condition

In this section effect of boundary condition on the buckling behaviour of the MEE plate is investigated. Three different boundary conditions are studied and their effects on buckling loads and corresponding mode shapes are
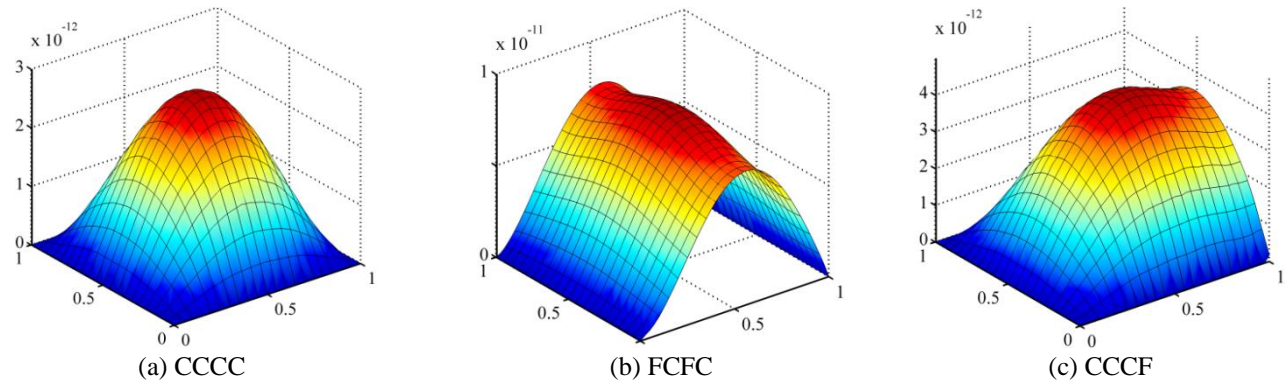
(a) CCCC   (b) FCFC   (c) CCCF

Fig. 13 Static deflection (in meters) of BFB MEE plate subjected to sinusoidal load

(a) CCCC   (b) FCFC   (c) CCCF
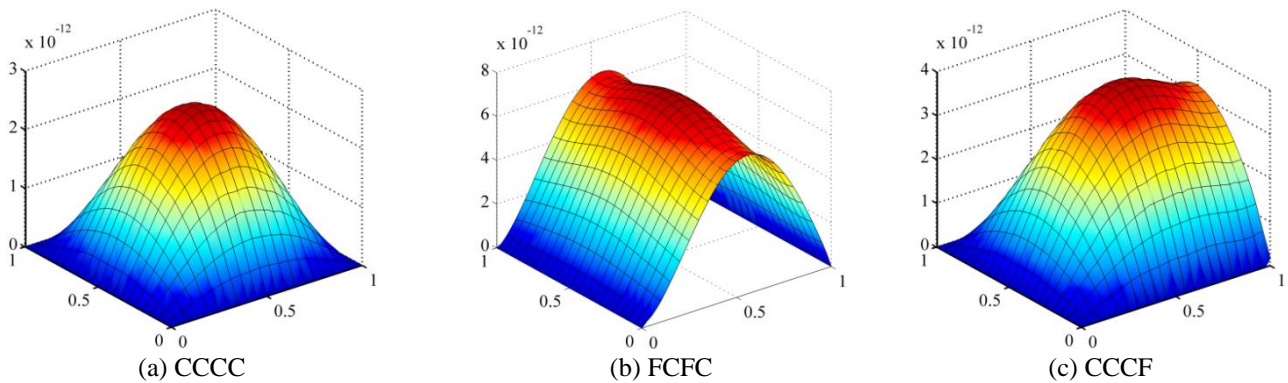
Fig. 14 Static deflection (in meters) of FBF MEE plate subjected to sinusoidal load
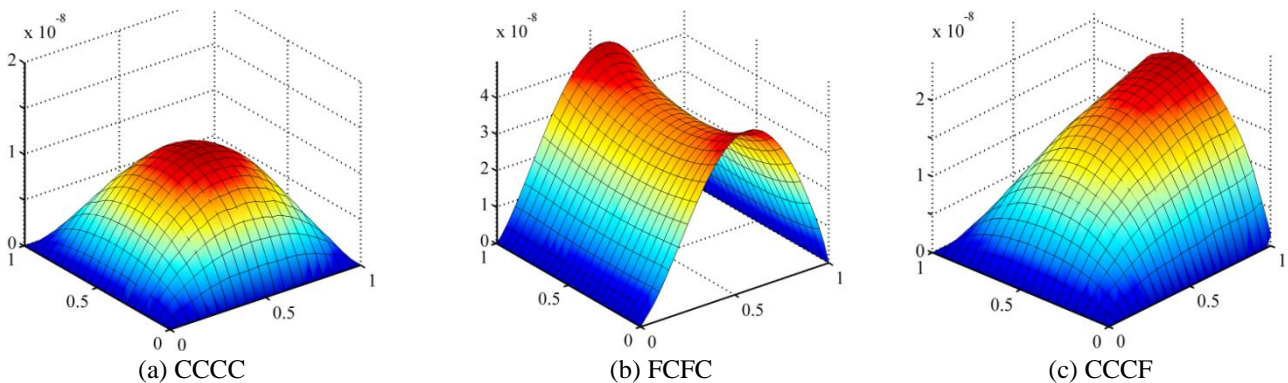

(a) CCCC   (b) FCFC   (c) CCCF

Fig. 15 Static deflection (in meters) of BFB MEE plate subjected to uniformly distributed load (UDL)

assessed. Fig. 11 presents the buckling loads and corresponding mode shapes for CCCC, CCCF and FCFC boundary condition. It can be noted that the largest buckling load is obtained for the most constrained CCCC plate and the lowest for the least constrained FCFC plate. Additionally, the effect of different boundary conditions is highlighted via corresponding mode shapes.

3.2 Static studies

The static deflection of MEE plate subjected to sinusoidal and uniformly distributed load (UDL) is studied for different boundary conditions. Firstly, the deflection in w-direction for the simply supported MEE plate subjected to sinusoidal load has been studied for the purpose of validation. The results for the B/F/B and F/B/F MEE plate

in Figs. 12(a) and (b) are found to be in very good agreement with the results available in the literature (Moita *et al*. 2009). The static deflection for different boundary conditions of the B/F/B MEE plate subjected to sinusoidal load is presented in Figs. 13(a)-(c) while Figs. 14(a)-(c) depicts for the F/B/F MEE plate. Further, Figs. 15(a)-(c) and 16(a)-(c) illustrate the results for the B/F/B and F/B/F MEE plate subjected to UDL, respectively. The static deflection of the F/B/F plate is observed to be lower than the B/F/B plate for all the investigated boundary conditions.

4. Conclusions

The buckling analysis of multilayered MEE plate has been performed using finite element approach considering

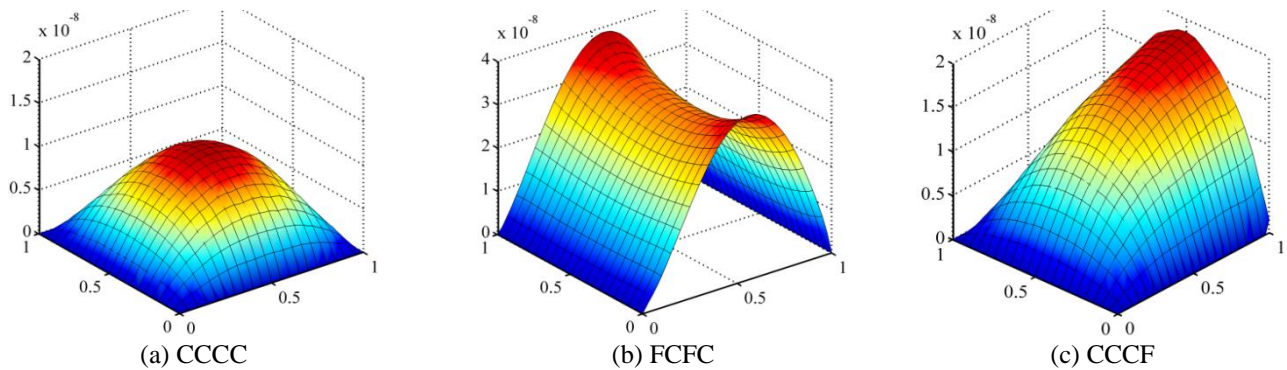(a) CCCC   (b) FCFC   (c) CCCF

Fig. 16 Static deflection (in meters) of FBF MEE plate subjected to uniformly distributed load (UDL)

the FSDT for displacement fields. The influence of boundary condition, aspect ratio, stacking sequence, span to thickness ratio and load factor was studied. For the evaluated effects of different parameters on critical buckling load and mode shapes, following conclusions could be drawn. Under the biaxial compression, the critical buckling loads halved in comparison with uniaxial compression and their corresponding mode shapes are also affected by the type of compression applied. Effect of stacking sequence is found to be significant with the F/B/F stacking sequence exhibiting larger buckling strength over B/F/B configuration. Further, buckling load decreased with increase in aspect ratio and span to thickness ratio of the MEE plate. Also, the highest constrained CCCC MEE plate witnessed largest buckling strength. In addition, the effect of load factor also exhibited a significant influence on critical buckling load. For all the considered boundary conditions, the studies concerned to static behaviour FBF plate realized the lowest deflection in the thickness direction.

References

Ansari, R. and Gholami, R. (2016), "Size-dependent buckling and postbuckling analyses of first- order shear deformable magneto-electro-thermo elastic nanoplates based on the nonlocal elasticity theory", *Int. J. Struct. Stab. Dyn.*, **10**, 1750014.

Bhangale, R.K. and Ganesan, N. (2006). "Static analysis of simply supported functionally graded and layered magneto-electro-elastic plates", *Int. J. Solid. Struct.*, **43**, 3230-3253.

Boomgaard, V. J. and Born, R. (1978), "A sintered magnetoelectric composite material BaTiO$_3$-Ni (Co, Mn)Fe$_2$O$_4$", *J. Mater. Sci.*, **13**(7), 1538-48.

Bouazza, M., Lairedj, A., Benseddiq, N. and Khalki, S. (2016), "A refined hyperbolic shear deformation theory for thermal buckling analysis of cross-ply laminated plates", *Mech. Res. Commun.*, **73**, 117-126.

Buchanan, G.R. (2004), "Layered versus multiphase magneto-electro-elastic composites", *Compos. B Eng.*, **35**(5), 413-420.

Chen J.Y., Heyliger P.R. and Pan, E. (2014), "Free vibration of three-dimensional multilayered magneto-electro-elastic plates under clamped/free boundary conditions", *J. Sound Vib.*, **333**, 4017-4029.

Ebrahimi, F. and Barati, M.R (2016e), "Static stability analysis of smart magneto-electro-elastic heterogeneous nanoplates embedded in an elastic medium based on a four-variable refined plate theory", *Smart Mater. Struct.*, **25**, 105014.

Ebrahimi, F., Dabbagh, A. and Barati, M.R. (2016), "Wave propagation analysis of a size-dependent magneto-electro-elastic heterogeneous nanoplate", *Eur. Phys. J Plus*, **131**(12), 433.

Ebrahimi, F. and Barati, M.R. (2016b), "Nonlocal Thermal Buckling Analysis of Embedded Magneto-Electro-Thermo-Elastic Nonhomogeneous Nanoplates", *IJST-T Mech. Eng.*, **40**(4), 243-264.

Ebrahimi, F., Jafari, A. and Barati, M.R. (2016), "Free Vibration Analysis of Smart Porous Plates Subjected to Various Physical Fields Considering Neutral Surface Position", *Arab. J. Sci. Eng.*, 1-17.

Ebrahimi, F. and Barati, M.R. (2016c), "Magneto-electro-elastic buckling analysis of nonlocal curved nanobeams", *Eur. Phys. J Plus*, **131**(9), 346.

Ebrahimi, F. and Barati, M.R. (2017), "Vibration analysis of smart piezoelectrically actuated nanobeams subjected to magneto-electrical field in thermal environment", Journal of Vibration and Control, Doi: 10.1177/1077546317708105.

Ebrahimi, F. and Barati, M.R. (2016d), "Buckling analysis of piezoelectrically actuated smart nanoscale plates subjected to magnetic field", *J. Intell. Mater. Syst. Struct.*, Doi: 10.1177/1045389X16672569.

Ebrahimi, F. and Barati, M.R. (2016a), "A unified formulation for dynamic analysis of nonlocal heterogeneous nanobeams in hygro-thermal environment", *Appl. Phys. A*, **122**(9), 792.

Farajpour, A. and Rastgoo, A., (2017), "Size-dependent static stability of magneto-electro-elastic CNT/MT-based composite nanoshells under external electric and magnetic fields", *Microsyst. Technol.*, **23**(12), 1-18.

Farajpour, A., Yazdi, M.H., Rastgoo, A., Loghmani, M. and Mohammadi, M. (2016) "Nonlocal nonlinear plate model for large amplitude vibration of magneto-electro-elastic nanoplates", *Compos. Struct.*, **140**, 323-336.

Grover, N., Maiti, D.K. and Singh, B.N. (2014), "An efficient C^0 finite element modeling of an inverse hyperbolic shear deformation theory for the flexural and stability analysis of laminated composite and sandwich plates", *Finite Elem. Anal. Des.*, **80**, 11-22.

Jadhav, P. and Bajoria, K. (2013), "Stability analysis of piezoelectric FGM plate subjected to electro-mechanical loading using finite element method", *Int. J. Appl. Sci. Eng.*, **11**(4), 375-391.

Jamalpoor, A., Ahmadi-Savadkoohi, A. and Hosseini-Hashemi, S. (2016), "Free vibration and biaxial buckling analysis of magneto-electro-elastic microplate resting on visco-Pasternak substrate via modified strain gradient theory", *Smart Mater. Struct.*, **25**(10), 105035.

Kattimani, S.C. and Ray, M.C. (2015), "Control of geometrically nonlinear vibrations of functionally graded Magneto-electro-elastic plates", *Int. J. Mech. Sci.*, **99**, 154-167.

Kattimani, S.C. and Ray, M.C. (2014a), "Smart damping of geometrically nonlinear vibrations of magneto-electro-elastic plates", *Compos. Struct.*, **114**, 51-63.

Kattimani, S.C. and Ray, M.C. (2014b), "Active control of large amplitude vibrations of smart magneto-electro-elastic doubly curved shells", *Int. J. Mech. Mater. Des.*, **10**, 351-378.

Kattimani S.C (2015), "Active control of geometrically nonlinear vibrations of Magneto-Electro-Elastic plates and dhells", Ph.D. Dissertation, IIT Kharagpur, India.

Ke, L.L., Wang, Y.S., Yang, J. and Kitipornchai, S. (2014), "Free vibration of size-dependent magneto-electro-elastic nanoplates based on the nonlocal theory", *Acta Mech. Sinica*, **30**(4), 516-525.

Kulkarni, K., Singh, B.N. and Maiti, D.K. (2015), "Analytical solution for bending and buckling analysis of functionally graded plates using inverse trigonometric shear deformation theory", *Compos. Struct.*, **134**, 147-157.

Kumaravel, A., Ganesan, N. and Sethuraman, R. (2007), "Buckling and vibration analysis of layered and multiphase magneto-electro-elastic beam under thermal environment", *Multidisc. Model. Mater. Struct.*, **3**(4), 461-476.

Lage, R.G., Soares, C.M.M., Soares, C.A.M. and Reddy, J.N. (2004), "Layerwise partial mixed finite element analysis of magneto-electro-elastic plates", *Comput. Struct.*, **82**, 1293-301.

Lang, Z. and Xuewu, L. (2013), "Buckling and vibration analysis of functionally graded magneto-electro-thermo-elastic circular cylindrical shells", *Appl. Math. Model.*, **37**(4), 2279-2292.

Li, Y.S., Cai, Z.Y. and Shi, S.Y. (2014), "Buckling and free vibration of magnetoelectroelastic nanoplate based on nonlocal theory", *Compos. Struct.*, **111**(1), 522-529.

Li, Y.S. (2014), "Buckling analysis of magnetoelectroelastic plate resting on Pasternak elastic foundation", *Mech. Res. Commun.*, **56**, 104-114.

Li, Y.S., Ma, P. and Wang, W. (2016), "Bending, buckling, and free vibration of magnetoelectroelastic nanobeam based on nonlocal theory", *J. Intell. Mater. Syst. Struct.*, **27**(9), 1139-1149.

Liu, J., Zhang, P., Lin, G., Wang, W. and Lu, S. (2016a), "Solutions for the magneto-electro-elastic plate using the scaled boundary finite element method", *Eng. Anal. Bound. Elem.*, **68**, 103-114.

Liu, J., Zhang, P., Lin, G., Wang, W. and Lu, S. (2016b), "High order solutions for the magneto-electro-elastic plate with non-uniform materials", *Int. J. Mech. Sci.*, **115**, 532-551.

Liu, M.F and Chang, T.P (2010), "Closed form expression for the vibration problem of transversely isotropic magneto-electro-elastic plate", *ASME J. Appl. Mech.*, **77**, 24502-10.

Luccioni, L.X. and Dong, S.B. (1998), "Levy-type finite element analyses of vibration and stability of thin and thick laminated composite rectangular plates", *Compos. B Eng.*, **29B**, 459-475.

Milazzo, A. (2016), "Unified formulation for a family of advanced finite elements for smart multilayered plates", *Mech. Adv. Mater. Struct.*, **23**(9), 971-980.

Moita, J., Soares, C.M.M. and Soares, C.A.M. (1996), "Buckling behaviour of laminated composite structures using a discrete higher-order displacement model", *Compos. Struct.*, **35**(1), 75-92.

Pan, E. (2001), "Exact solution for simply supported and multilayered magneto-electroelastic plates", *J. Appl. Mech.-T.*, **68**, 608-618.

Pan, E. and Heyliger, P.R. (2002), "Free vibration of simply supported and multilayered magnetoelectro-elastic plates", *J. Sound Vib.*, **252**(3), 429-442.

Pan, E. and Heyliger, P.R. (2003), "Exact solutions for magneto-electro-elastic laminates in cylindrical bending", *Int. J. Solid. Struct.*, **40**(24), 6859-6876.

Pan, E. and Han F. (2005), "Exact solutions for functionally graded and layered magneto-electro-elastic plates", *Int. J. Eng.*

Sci., **43**, 321-339.

Ramirez, F., Heyliger, P.R. and Pan, E. (2006), "Free vibration response of two-dimensional magneto-electro-elastic plates", *J. Sound Vib.*, **292**, 626-644.

Ray, M.C., Bhattacharya, R. and Samanta, B. (1994), "Static analysis of an intelligent structure by the finite element method", *Comput. Struct.*, **52**, 617-631.

Razavi, S. (2017), "On the buckling the behavior of a multiphase smart plate based on a higher-order theory", *Mech. Adv. Compos. Struct.*, **4**(1), 47-58.

Reddy, J.N. (2004), *Mechanics of Laminated Composite Plates and Shells: Theory and Analysis*, CRC Press, LLC.

Rogowski, B. (2015), "The transient analysis of a conducting crack in magneto-electro-elastic half-space under anti-plane mechanical and in-plane electric and magnetic impacts", *Arch. Appl. Mech.*, **85**(1), 29-50.

Simoes Moita, J.M., Mota Soares, C.M. and Mota Soares, C.A. (2009), "Analyses of Magneto-electro-elastic plates using a higher order finite element model", *Compos. Struct.*, **91**, 421-426.

Sladek, J., Sladek, V., Kharulec, S. and Pan, E. (2013), "Analyses of functionally graded plates with magnetoelectroelasic layer", *Smart Mater. Struct.*, **22**, 035003.

Sreehari, V.M., George, L.J. and Maiti, D.K. (2016), "Bending and buckling analysis of smart composite plates with and without internal flaw using an inverse hyperbolic shear deformation theory", *Compos. Struct.*, **138**, 64-74.

Thai, H.T and Vo, T.P. (2013), "A new sinusoidal shear deformation theory for bending, buckling, and vibration of functionally graded plates", *Appl. Math. Model.*, **37**(5), 3269-81.

van Suchtelen, J. (1972), "Product properties: a new application of composite materials", *Philips Res. Rep.*, **27**, 28-37.

Vinyas, M. and Kattimani, S.C. (2017a), "Static studies of stepped functionally graded magneto-electro-elastic beam subjected to different thermal loads", *Compos. Struct.*, **163**, 216-237.

Vinyas, M. and Kattimani, S.C. (2017b), "Finite element based assessment of static behaviour of multiphase magneto-electro-elastic beam under different thermal loading", *Struct. Eng. Mech.*, **62**(5), 519-535.

Viun, O., Loboda, V. and Lapusta, Y. (2016), "Electrically and magnetically induced Maxwell stresses in a magneto-electro-elastic medium with periodic limited permeable cracks", *Arch. Appl. Mech.*, **86**(12), 2009-2020.

Vuksanović, D. (2000), "Linear analysis of laminated composite plates using single layer higher-order discrete models", *Compos. Struct.*, **48**, 205-211.

Wu, C.P., Chen, S.J. and Chiu, K.H. (2010), "Three-dimensional static behavior of functionally graded magneto-electro-elastic plates using the modified Pagano method", *Mech. Res. Commun.*, **37**(1), 54-60.

Xin, L. and Hu, Z. (2015), "Free vibration of simply supported and multilayered magneto-electro-elastic plates", *Compos. Struct.*, **121**, 344-350.

Zhou, K., Li, Y.D. and Liu, S.L. (2016), "Effects of the volume fraction of piezoelectric particles in the magneto-electro-elastic interfacial region on the fracture behavior of a laminate multiferroic plate", *Acta Mech.*, **228**(4), 1229-1248.

CC

Appendix

The nodal strain-displacement matrices $[b_{bt}]$, $[b_{br}]$, $[b_{st}]$ and $[b_{sr}]$ appearing in the Eq. (21) are given by

$$[b_{bt}] = [b_{bt1} \ b_{bt2} \ b_{bt3} \ b_{bt4}], \quad [b_{br}] = [b_{br1} \ b_{br2} \ b_{br3} \ b_{br4}],$$

$$[b_{st}] = [b_{st1} \ b_{st2} \ b_{st3} \ b_{st4}] \text{ and } [b_{sr}] = [b_{sr1} \ b_{sr2} \ b_{sr3} \ b_{sr4}]$$

The various sub-matrices $[b_{tbi}]$, $[b_{rbi}]$, $[b_{tsi}]$ and $[b_{rsi}]$ (i=1, 2, 3, 4) are as follows

$$[b_{bti}] = \begin{bmatrix} \dfrac{\partial n_i}{\partial x} & 0 & 0 \\ 0 & \dfrac{\partial n_i}{\partial y} & 0 \\ 0 & 0 & 0 \\ \dfrac{\partial n_i}{\partial y} & \dfrac{\partial n_i}{\partial x} & 0 \end{bmatrix}, \quad [b_{bri}] = \begin{bmatrix} \dfrac{\partial n_i}{\partial x} & 0 \\ 0 & \dfrac{\partial n_i}{\partial y} \\ \dfrac{\partial n_i}{\partial y} & \dfrac{\partial n_i}{\partial x} \end{bmatrix},$$

$$[b_{sti}] = \begin{bmatrix} 0 & 0 & \dfrac{\partial n_i}{\partial x} \\ 0 & 0 & \dfrac{\partial n_i}{\partial y} \end{bmatrix} \text{ and } [b_{sri}] = \begin{bmatrix} n_i & 0 \\ 0 & n_i \end{bmatrix}.$$